Nano-structured Hydrotrope-Caged Cytochrome c with Boosted Stability in Harsh Environments: A Molecular Insight

Pranav Bharadwaj[†, ϕ], Dheeraj Kumar Sarkar[§, ψ, ϕ], Meena Bisht[‡], Sachin M. Shet[†], S. K. Nataraj,[†] Veeresh Lokesh[‡], Gregory Franklin*[,‡], Jan Brezovsky*[,§, ψ], and Dibyendu Mondal*[,†,‡]

† Centre for Nano and Material Sciences, Jain University, Bangalore 562112, India.

§ Laboratory of Biomolecular Interactions and Transport, Department of Gene Expression, Institute of Molecular Biology and Biotechnology, Faculty of Biology, Adam Mickiewicz University, Uniwersytetu Poznanskiego 6, 61-614 Poznan, Poland

ψ International Institute of Molecular and Cell Biology in Warsaw, Ks Trojdena 4, 02-109 Warsaw, Poland

‡ Institute of Plant Genetics (IPG), Polish Academy of Sciences, Strzeszyńska 34, 60-479 Poznań, Poland

*Corresponding authors

ϕ These authors have contributed equally to this work.

ABSTRACT: Green and nano-structured catalytic media are vital for bio-catalysis to attenuate the denaturation tendency of biocatalysts under severe reaction conditions. Hydrotropes with multi-faceted physiochemical properties represent promising systems for sustainable protein packaging. Herein, the suitability of adenosine-5'-triphosphate (ATP) and cholinium salicylate ([Cho][Sal]) ionic liquid (IL) to form nano-structures and to nano-confine Cytochrome c (Cyt c) were demonstrated to enhance the stability and activity under multiple stressors. Experimental and computational validations were undertaken to explain the nano-structured phenomenon of ATP and IL, structural organizations of nano-confined Cyt c, and site-specific interactions that stabilize the protein structure. Both ATP and IL form nano-structures in aqueous media and could cage Cyt c via multiple nonspecific soft interactions. Remarkably, the engineered molecular nano-cages of ATP (5-10 mM), IL (300 mg/mL), and ATP+IL surrounding Cyt c resulted in 9-to-72-fold higher peroxidase activity than native Cyt c with exceptionally high thermal tolerance (110°C). The polar interactions with the cardiolipin binding site of Cyt c, mediated by hydrotropes, were well correlated with the increased peroxidase activity. Furthermore, higher activity trends were observed in the presence of urea, GuHCl, and trypsin without any protein degradation. Specific binding of hydrotropes in highly mobile regions of Cyt c (Ω 40-54 residues) and enhanced H-bonding with Lys and Arg offered excellent stability under extreme conditions. Additionally, ATP effectively counteracted reactive oxygen species (ROS)-induced denaturation of Cyt c, which was enhanced by the [Sal] counterpart of IL. Overall, this study explored the robustness of nano-structured hydrotropes to have a higher potential for protein packaging with improved stability and activity under extreme conditions. Thus, the present work highlights a novel strategy for real-time industrial bio-catalysis to protect mitochondrial cells from ROS-instigated apoptosis.

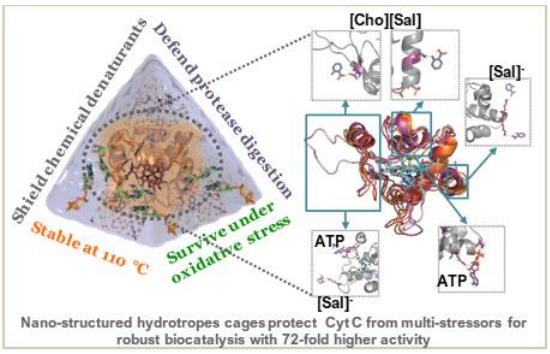

INTRODUCTION

Adenosine-5'-triphosphate (ATP) has shown multi-faceted functions, including its participation in the electron transport chain, acting as the energy currency of cells, holding the key for caspase-9-activated apoptosis, and taking part in transcription by revamping chromatin complexes.[1-3] The role of physiological concentrations of ATP in preventing thermally-induced protein aggregation in mammalian cells was previously demonstrated by *Nguyen and Benusaude*,[4] and the answer regarding the regulation of a high concentration of ATP (2-10 mM) in the cell was unveiled by *Patel and co-workers,* whereby ATP is claimed as a biological hydrotrope.[5] The term 'hydrotrope' was coined by *Neuberg* for amphiphilic molecules having a characteristic range of minimum hydrotrope concentration, which augment the solubility of partially soluble organic or hydrophobic substances in water.[6-7] This opened a new channel to explore ATP in the medicinal field to treat Parkinson's and Alzheimer-like diseases by preventing phase separation of biological fluids, which causes amyloid

fibrillation.[8-9] The solubilizing tendency of ATP was attributed to its nonspecific aggregation, charge reinforcement, and self-assembly through hydrophobic interactions (Figure 1a).[10-11] Thus, the hydrotropic mechanism of ATP follows both the Neuberg and Hofmeister effects.[12] Self-aggregated ATP is found to provide thermal stability to lysozyme, malate dehydrogenase, and ubiquitin,[13] and so it is important to understand how the self-aggregation property of ATP is useful in protein packaging under multiple stressors, which has not been previously studied.

Unlike ATP, various amphiphilic nano-structured solvents have recently emerged with promising applications in energy-efficient bioprocesses.[14] Due to their highly manipulative nature, ionic liquids (ILs) have gained interest for their ability to increase enzyme solubility and thermal stability.[15] Interestingly, bio-based ILs of the cholinium family have shown hydrotropic properties[16] with greater hydrophobicity and can enhance the nano-structuring of amphiphilic solutes in aqueous media.[17] Earlier reports have shown cholinium-based ILs for protein packaging with long-term stability and activity,[15] but there is a lack of understanding of the underlying mechanisms by which hydrotropic ILs (potential amphiphilic molecules) can regulate protein stability and activity.[18] In this regard, an IL with a salicylate counterpart caught our attention as it contains carboxylic and hydroxyl groups, along with a hydrophobic aromatic ring featuring the salicylate ion and showing multiple interaction sites in the aqueous medium (Figure 1b).[19-20] Additionally, salicylic acid is an important phytohormone that alters the mitochondrial processes by amplifying the concentration of reactive oxygen species (ROS) and induces cells to undergo programmed cell death.[21-22] During apoptosis, ATP plays a crucial role in caspase-9 activation, a process stimulated by cytochrome c (Cyt c) release from mitochondria.[23] Since both ATP and salicylate are coupled to Cyt c, the latter was chosen as a model protein for this study (Figure 1c), and ATP and choline salicylate ([Cho][Sal]) IL as the nano-structured hydrotropes.

Cyt c is a mitochondrial-based 13 kDa monomeric protein comprising approximately 104 residues and is widely distributed across eukaryotes, bacteria, and archaea.[24] Despite its significant role in electron transfer, this protein is of great interest in many technological applications like biosensors, synthetic receptors, and molecular imprinting among others.[24] Cyt c also shows peroxidase-like activity and serves as a bio-catalyst in several catalytic transformations.[24] The protein is highly vulnerable to denaturation under prevailing stress conditions such as extreme temperatures, oxidative stress, and proteolytic and chemical denaturants.[25] Recently, a surface modification strategy using quantum dots, metal-organic frameworks,[26], and DNA was reported to enhance the stability of Cyt c.[25,27] However, the stability of the protein when confined within a hydrotrope system has not yet been reported. Considering the hydrotropism and probability of nano-structuring,[24] the present study aimed to cage Cyt c in ATP and [Cho][Sal] IL-based hydrotropes, and thereby improve the activity and stability of the protein in gentle and harsh environments (such as high temperature, chemical denaturants, protease digestion, and oxidative stress). Therefore, detailed experimental and *in silico* approaches were undertaken to study the structure-function relationship of nano-confined Cyt c in ATP, [Cho][Sal] and ATP + IL at a molecular level to develop a novel and sustainable solvent manipulation strategy for dynamic protein packaging and robust bio-catalysis.

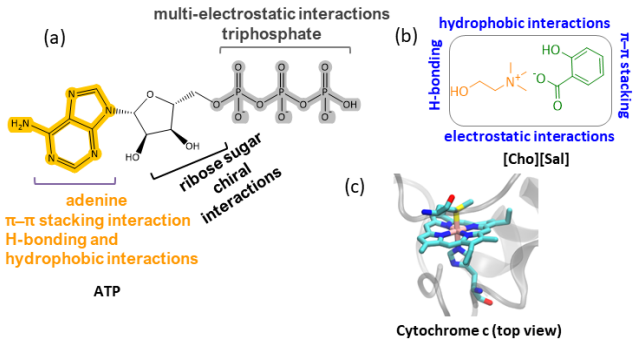

Figure 1: Chemical structures and structural features of (a) ATP and (b) [Cho][Sal] IL, with possible interaction sites. (c) The modeled active site structure of Cyt c, based on the crystallographic structure of bovine heart Cyt c (PDB code: 2B4Z) at 1.5 Å resolution.

RESULTS AND DISCUSSION

ATP and [Cho][Sal] IL as nano-structured hydrotropes

To understand the extent to which the IL affects the self-aggregation of ATP, which is vital for its role as a biological hydrotrope, we performed molecular dynamics (MD) simulations of 5 mM ATP, 300 mg/mL [Cho][Sal], and their mixture. The pair-wise interactions of ATP and [Cho][Sal] molecules in water and the mixture were investigated using radial distribution functions (RDF). As expected, ATP exhibited a self-aggregating tendency at 4-to-5 Å and up to 15 Å (Figure 2a). The self-aggregating propensity of ATP molecules from a chemical perspective in the presence of an IL can occur in three possible ways, first the anion-π interactions between the aromatic ring and negatively charged oxygen moiety of phosphate groups, secondly through a non-bonding aromatic ring interaction (H-bonding, π–π stacking interactions, and cation–π interactions) and third, H-bond formation between the sugar and triphosphate group.[11] It was evident from our analysis that two ATP molecules preferentially formed stack-like configurations in water (Figure S1a). In the presence of [Cho][Sal], the IL-mediated H-bonding (Figure S1b) markedly decreased the occurrence of the stack-like configurations of ATP, thereby increasing the multi-faceted nature of ATP self-aggregation (Figure 2b). Notably, we found that the IL at a molecular concentration of 300 mg/mL increases the H-bonding network mediated by cholinium or salicylate (Figure S1c). Unsurprisingly, we have not observed any perturbation of the [Cho][Sal] nano-structure upon the addition of ATP, given its low concentration. In addition to RDFs, the self-aggregating behavior of ATP and

ATP+IL was further verified by a concentration-dependent ζ-potential study (Figure 2c and Figure S2). At 1 mM concentration, which is below the critical hydrotropic concentration (2 mM), a single broad distribution peak was observed with maxima of -8.12 mV, indicating the existence of a single non-aggregated structure (Figure 2c). At 2.5 mM, the distribution curve shifted to a lower negative value with peak maxima of -5.96 mV. This lowering in the ζ-potential indicates the beginning of aggregated structures similar to the self-aggregation of nano-particles as a result of the decrease in the electrophoretic mobility.[28]

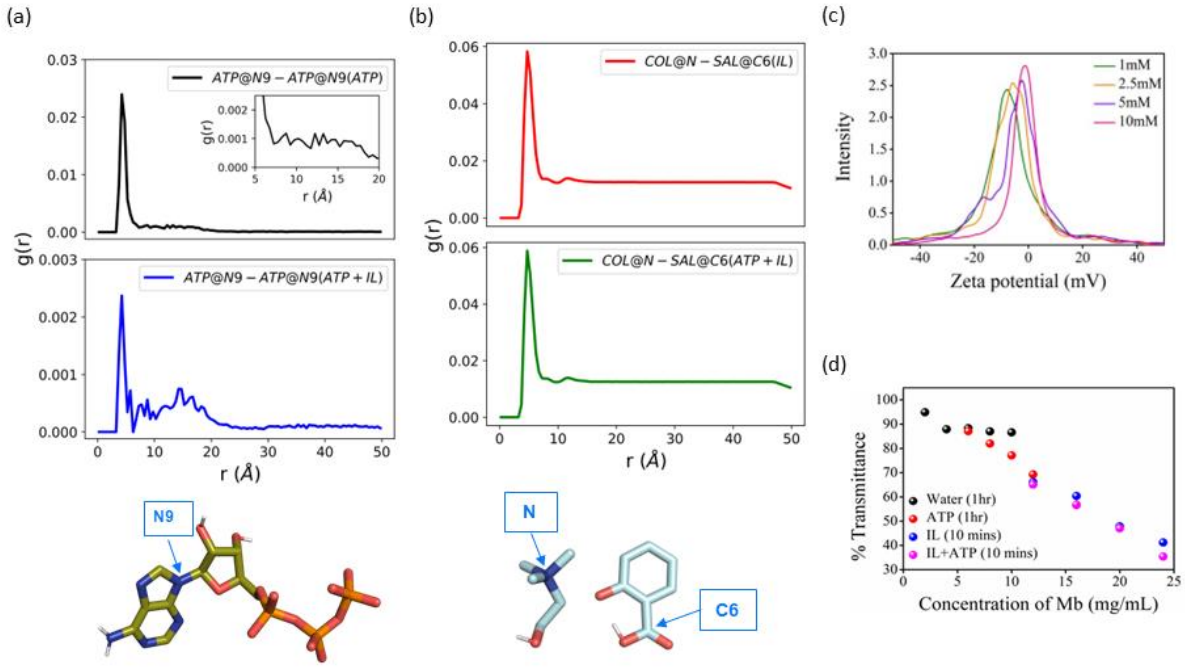

Figure 2: **Mutual effects of ATP and [Cho][Sal] on their respective nano-structure and interactions**. (a) RDF of 5 mM ATP (black) and 5 mM ATP in presence of [Cho][Sal] (blue). The N9 atom of ATP used for RDF calculation is shown by the blue arrow. (b) RDF of 300 mg/mL [Cho][Sal] (red) and [Cho][Sal] with added ATP (green). The N and C6 atoms used for RDF calculation are shown by the blue arrows. (c) Concentration-dependent Zeta potential analysis of ATP. (d) solubility data of equine heart myoglobin in an aqueous medium at pH 7 in the presence and absence of 5 mM ATP, 100 mg/mL [Cho][Sal], and a combination of both ATP+IL.

This is further evidenced by the shift of maxima from -5.96 to -2.35 mV for 5 mM ATP. Finally, at 10 mM concentration, a broad single peak with maxima at -1.42 mV was obtained, which indicates the presence of a self-assembled, nano-structured ATP state. Conversely, 200mg/mL of [Cho][Sal] shows a very broad Gaussian peak with a maximum at -9.12 mV (Figure S3), which shifts to a lower value of -4.02 mV in the presence of 5 mM ATP, justifying the hypothesis that the IL enhanced the self-assembly of amphiphiles.[19] The hydrodynamic radius (R_h) of 5 mM ATP was found to be 0.83 nm (slightly higher than R_h of monomeric ATP, which is 0.57-0.65 nm),[10] suggesting the existence of nano-structured/oligomeric forms and supporting our earlier evidence. In the presence of the IL, the R_h of ATP increased to 1.12 nm (Figure S4). To demonstrate the hydrotropic property of ATP and [Cho][Sal], solubility studies of myoglobin (Mb) were carried out in an aqueous medium at pH 7 in the presence and absence of 5 mM ATP, 100 mg/mL IL and a combination of both (Figure 2d). After 1hr, the maximum solubility of Mb was found to be 6 mg/mL. In contrast, ATP-induced solubility of Mb increased to 16 mg/mL during the same duration, which directly shows the hydrotropic nature of ATP. In the case of [Cho][Sal], the same solubility was achieved within 5 mins. Thus, the concentration of Mb was further increased and examined until 24 mg/mL. Interestingly, for ATP+IL, 24 mg/mL Mb showed higher solubility than the IL-only medium. These observations of enhanced solubility in the presence of two hydrotropes inspired us towards nano-confinement of Cyt c using ATP and [Cho][Sal]-based nano-structured hydrotropes to enable improved biological activity and stability of the protein.

Structural features of nano-structured hydrotrope-caged Cyt c

To understand the structural features of caged Cyt c, four molecular systems were prepared, namely keeping Cyt c in water, ATP, IL, and both ATP + IL at 26.85°C (Figure 3a-d). The RDFs of hydrotropes in all systems with and without the presence of the protein were in agreement, indicating that the presence of Cyt c had a negligible effect on the adopted hydrotrope nano-structures (Figure 2a,b & Figure S5). A lower dielectric constant of the protein or more negative zeta potential of ATP and IL can be related to the colloidal stability of caged Cyt C. Accordingly, ζ-potential analysis was employed to envisage the electrostatic interaction between Cyt c and nano-structured hydrotropes.

We found the ζ-potential of native Cyt c solution (10 μM) to be +1.24 mV (Figure 3e), and the ζ-potential of ATP (5 mM), IL (200 mg/mL), and ATP+IL was -2.48 mV, -9.16 mV, and -4.09 mV, respectively. After Cyt c incubation with ATP, IL, and IL+ATP, the ζ-potential values decreased to -1.66 mV, -6.64 mV, and -3.46 mV, respectively (Figure 3e). These changes in the ζ-potential demonstrate the possible electrostatic interaction between the protein and the nano-structured hydrotropes. At a lower concentration of Cyt c (2 μM), the ζ-potential of ATP increased from -2.48 mV to -4.38 mV, indicating the reorganization of a self-assembled ATP nano-structure around Cyt c (Figure S6).
Further R_h of native Cyt c was found to be 1.25 nm, which agrees with a previous report[30], and in the presence of ATP, the value increased to 1.99 nm showing self-assembly of ATP around the protein (Figure 3f and Figure S7). In the presence of IL+ATP, R_h of Cyt c is further increased to 2.22 nm. Thus, the hydrotropic mechanism of ATP occurs initially by charge reinforcement, followed by the stacking phenomenon. Along with ζ-potential and DLS, structures of nano-confined Cyt c were further characterized by UV-vis spectra (Figure S8). UV-vis spectrum of pure Cyt c comprises a Soret (B-band), Q band, and a shoulder peak (N-band), altogether representing the structural morphology around the heme group (Figure S8). In the presence of 5 mM ATP, a hyperchromic shift (a blue shift of 2 nm) in the Soret band (409 nm) was observed, suggesting that a non-polar environment dominates around the heme. In the case of IL (300 mg/mL [Cho][Sal]), absorbance in the Soret band enhanced considerably together with a blue shift, while the Q-band (520-550 nm) is broadened due to enhanced absorbance. This suggests changes in the tertiary conformations. An additional broad peak can be seen in the range of 620-695 nm, the intensity of which increases with an increased concentration of IL, demonstrating the local stability induced by [Cho][Sal].[31] Moreover, the observed peaks suggest that a transit towards penta-coordinated Cyt c is formed in the presence of IL, leading to the formation of a high-spin Fe(III) heme center.[31] A hypochromic shift in the Soret band region was observed for Cyt c caged within both ATP and IL nano-structures, indicating that the stability offered by both the hydrotropic systems by derived from driving the protein core towards the non-polar region. Overall, it is evident that the self-aggregation propensities of the hydrotropes persisted even in the presence of Cyt c, and the structure of caged Cyt c was partially affected (without any unfolding, as discussed below) due to multiple interactions with nano-structured hydrotropes.

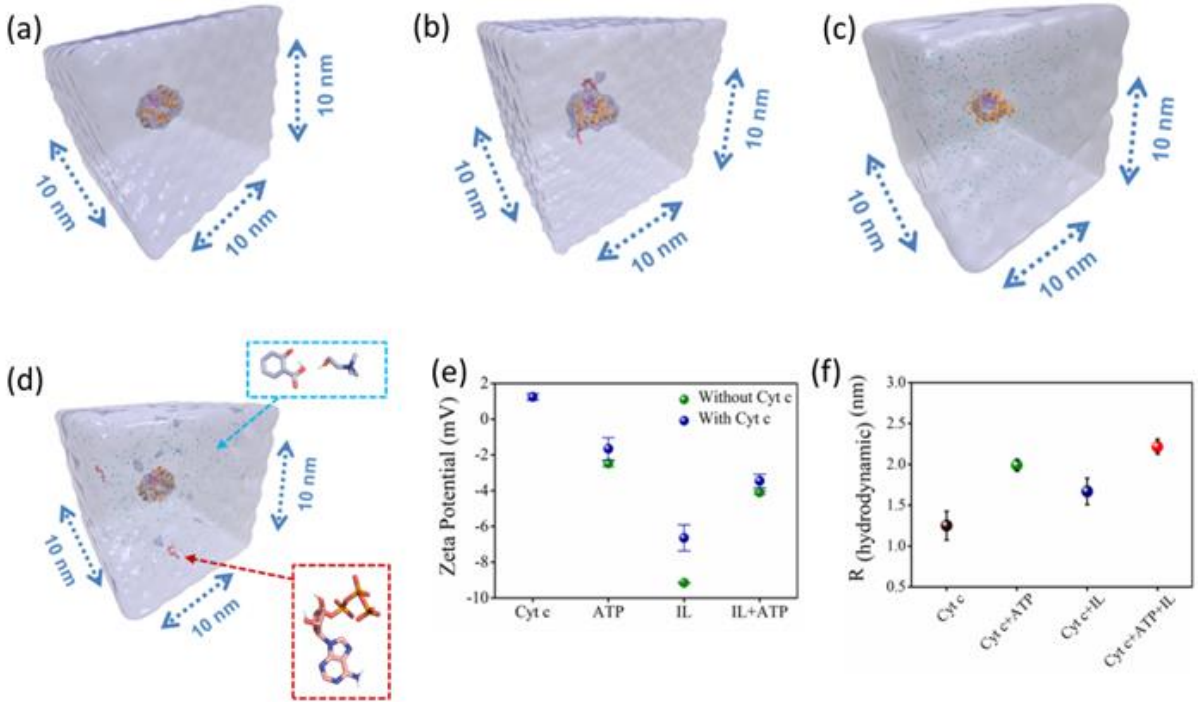

Figure 3: (a-d) Representative figures of a solvent of cubic box length 10 nm for Cyt c in H_2O (a), ATP+ H_2O (b), [Cho][Sal] + H_2O (c), and ATP + IL + H_2O molecular systems (d). Graph (e) shows zeta (ζ)-potential studies of nano-structured hydrotropes and Cyt c with and without nano-structured hydrotropes. Plot (f) depicts the hydrodynamic radius (R_h) of native Cyt c and Cyt c caged in different nano-structured hydrotropes.

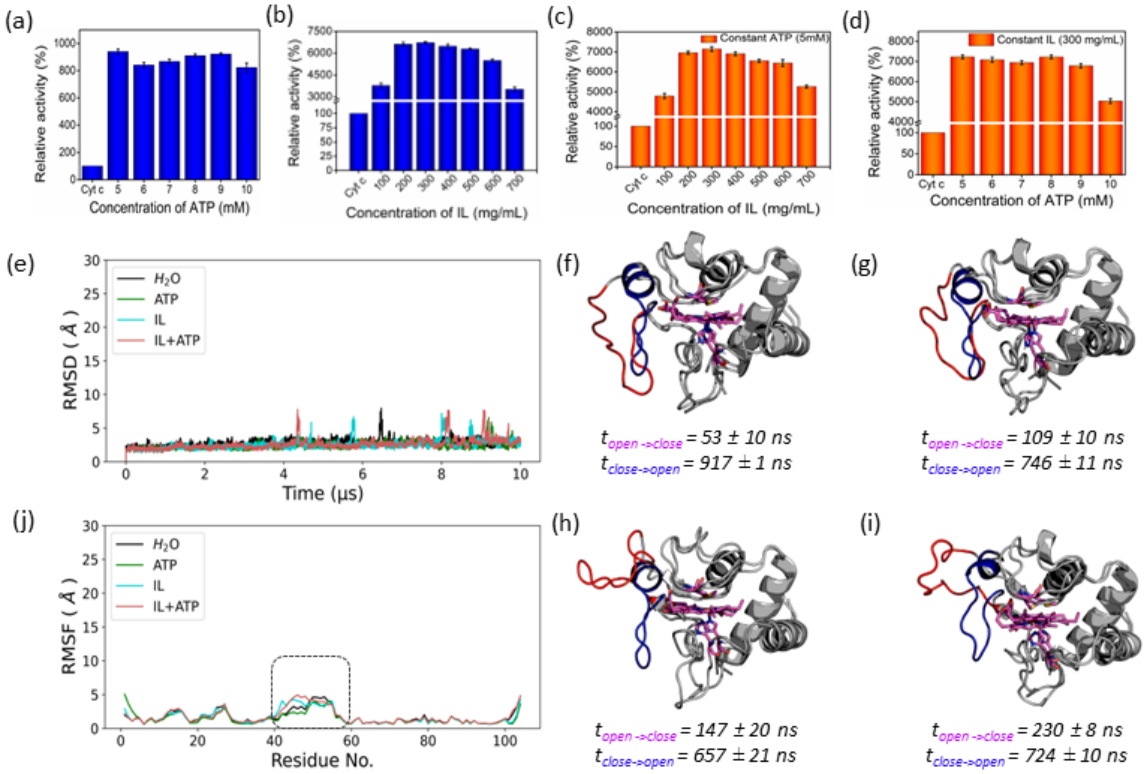

Figure 4: Peroxidase-like activity of Cyt linked to its dynamics. Optimization results of peroxidase-like activity of Cyt c with different hydrotropic concentrations of (a) ATP, (b) [Cho][Sal] IL, (c) varying [IL] by keeping [ATP] constant (5 mM), and (d) varying [ATP] by keeping IL constant (300 mg/mL). Structural characterization of Cyt c in four solvent systems at 26.85°C. (e) Stability and dynamics of Cyt c structure simulated in four solvent systems shown as backbone RMSD and RMSF, respectively. The peaks in the RMSD plot correspond to the reversible openings of Ω 40-54 residue region highlighted in the RMSF plot by a dashed rectangle. Figures (f-i) show the metastable states representing open (red) and closed (blue) structures of Cyt c in H_2O, ATP, IL, and ATP+IL, respectively. The timescales of opening and closing processes were calculated as mean first passage times between the two states presented as mean ± standard deviation.

Nano-structured hydrotrope-caged Cyt c with boosted peroxidase activity: molecular insights on the improved catalytic activity and enhanced stability

In the presence of H_2O_2, Cyt c undergoes covalent modifications, which facilitate peroxidase-like activity.[32] The activity of Cyt c in the presence of 5-10 mM ATP showed a similar trend with an >8-fold higher activity than native Cyt c (Figure 4a). Since a typical nano-structure is formed around Cyt c in the range of hydrotropic concentration (5-10 mM), similar relative activity is achieved rather than a maxima-minima trend. ATP acts as a hydrotrope initially by unwinding the protein and then stabilizing the extended chain through electrostatic interactions,[11] which may be a reason for the high peroxidase activity. In the case of the [Cho][Sal] IL, nearly the same relative activities were seen from the 200-to-500 mg/mL range (Figure 4b). A clear trend was observed with the highest relative activity of 67-fold at the concentration of the IL of 300 mg/mL. The activity data agree with the UV-vis absorption spectra that inferred the transition of Cyt c towards penta coordinated high spin complex. When the Met_{80} ligand is displaced, Cyt c naturally exhibits pronounced peroxidase-like activity.[32] Interestingly, a replica of the IL optimization trend pattern was observed when using the ATP+IL mixture when [ATP] was kept constant (5 mM) and IL was varied (Figure 4c). At 300 mg/mL IL and 5 mM ATP concentrations, the activity of Cyt c was enhanced 72-fold more than native Cyt c. This activity enhancement is indicative that the structure of Cyt c is still intact and combined hydrotropic systems boost the peroxidase activity further. Some ILs enhance the self-assembly of co-solutes in the media due to the virtue of their solvo-phobic effects.[17] Accordingly, the concentration of ATP was varied with IL being constant (300 mg/mL). A similar trend was observed with a >69-fold increase in activity (Figure 4d). These trends demonstrate that both IL and ATP further enhance the conformational changes of Cyt c, followed by stabilization of the extended protein structure by the self-assembling of ATP to surround it. Similar inference can be observed from Figure S5a (blue line), in which ATP tends to self-aggregate, even in the presence of IL and Cyt c.

To understand the behavior of nano-structured hydrotrope-caged Cyt c, adaptive sampling MD simulations with a total of 10 μs simulation time for each system were performed. In all systems, we observed reversible structural rearrangements of the protein backbone (Figure 4e), which could be traced to the reversible opening of the loop in the Ω 40-54 residue region that was relatively more mo-

bile than other parts of the protein for all four systems (Figure 4j). This region corresponds to the mAb 1D3 binding site and is reported to be more dynamic,[33] while having specificity towards Cytochrome c oxidase.[34]

To delineate the details of this process and its modulation by the action of nano-structured hydrotropes, we have constructed Bayesian Markov state models from the simulations. This inference revealed the presence of metastable states with an open conformation of the Ω 40-54 loop of Cyt c in all systems (Figures 4f-i), which were characterized by their increased RMSD and elevated radius of gyration (Figure S9). The interactions of ATP and IL with Cyt c resulted in marked effects on the stability and dynamics of this region. In the presence of ATP, the closing process was approximately 2 times slower, whereas the opening became approximately 20% faster (Figure 4g). Similarly, the presence of the IL resulted in a faster opening process, while the closing speed was slowed even more prominently than that observed for ATP (Figure 4h). Finally, the mixture of ATP and IL showed a synergistic effect on the dynamics of Cyt c, resulting in the slowest closing and faster opening in contrast to the water environment, enhancing the dynamics of this functionally important region (Figure 4i).

Since both ATP and IL were significantly affecting the dynamics of Cyt c, the residues exhibiting the most frequent H-bonding with hydrotropes were identified from the simulations (Figure 5a-c). In general, ATP interacted preferentially with Lys residues (Figure S10a), which is in accordance with an earlier report demonstrating that triphosphate group of ATP can deliver weak, nonspecific interactions with conserved Lys or Arg residues.[10] Additionally, the IL had a wide range of residues as binding partners, although Lys was the most populated in terms of H-bonding (Figure S10b). This trend was also maintained in the mixture of ATP and IL (Figure S10c).

We observed marked overlap in particular interaction hot spots for IL and ATP on the surface of Cyt c (Figure 5a-c, Figure S10d,e). ATP most often formed interactions with K13, K25, K27, K72, K86, and K87 (Figure S11a,c). Notably, K72 is involved in site A of Cyt c, which is crucial for interacting with cardiolipin,[35] and was reported to have a significant role in the peroxidase activity of Cyt c.[36] Conversely, IL demonstrated the highest affinity towards Y97 (Figure S11b,d) despite its general preference to Lys. Interestingly Y97 has been ascribed a significant role in keeping the terminal helix intact and hence providing structural stability to the protein.[37] Finally, these simulations also revealed variation in the secondary structures of native and caged Cyt c in the presence of IL, where the transition of turn to parallel beta-sheets was observed (Figure 5d).

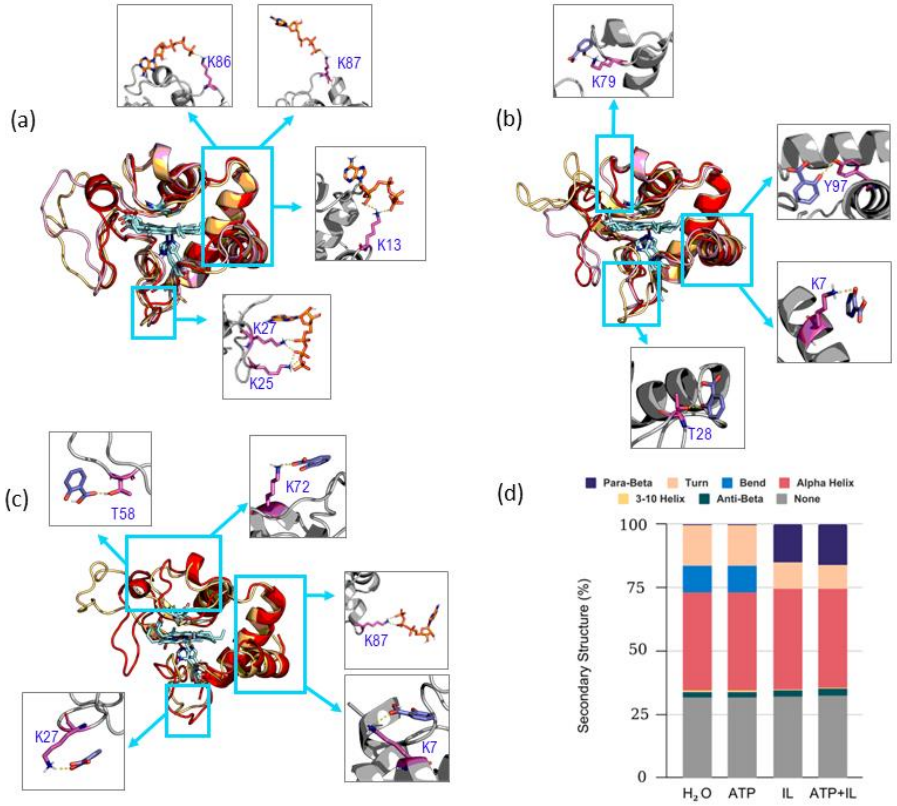

Figure 5: Interaction of hydrotrope molecules in metastable states in the open, closed, and transient Cyt c conformations from 10 μs of adaptive simulation data with (a) ATP, (b) [Cho][Sal] IL, and (c) ATP + IL. The top residues that have hydrogen bond interactions between solvent molecules and Cyt c are shown in gray squares (dashed), and the protein regions are highlighted in cyan (solid). Plot (d) shows the secondary structural changes of the four Cyt c systems we generated. All simulations were performed at 26.85°C. In all cases, the concentration of ATP and IL was 5 mM and 300 mg/mL, respectively.

Nano-structured hydrotrope-caged Cyt c with enhanced thermal stability for high-temperature bio-catalysis

The activity of Cyt c increases with temperature up to 70°C, above which the protein starts to denature gradually (Figure 6a). Above 80°C, the activity drops due to significant denaturation of the protein.[25] A similar trend is observed in the presence of ATP, but the activity extends to approximately a 20-fold increase than for native Cyt c at 70°C. In the case of IL and ATP+IL systems, the denaturation is prevented even up to extremes of 110°C. At 90°C, both Cyt c+IL and Cyt c+IL+ATP showed an accelerated activity value corresponding to 76-80-fold higher than native Cyt c. The stability aspects of Cyt c, when coupled to hydrotropes at elevated temperatures, were supported by UV-vis spectra (Figure 6b). Enhancement in the Soret band intensity was observed for both IL and IL+ATP at 90°C compared to the results obtained at 26.85°C, which implies that the secondary conformation, formed due to weak interactions between the hydrotrope systems and Cyt c, was preserved. ATP+IL showed an intensified Soret peak compared to the other conditions at 110°C, suggesting the advantage of engineering Cyt c with two different hydrotropes when aiming for high-temperature bio-catalysis. Additionally, as evident from non-reducing SDS-PAGE (Figure 6c), improved activity trends at high temperatures were achieved without structural degradation of the protein.

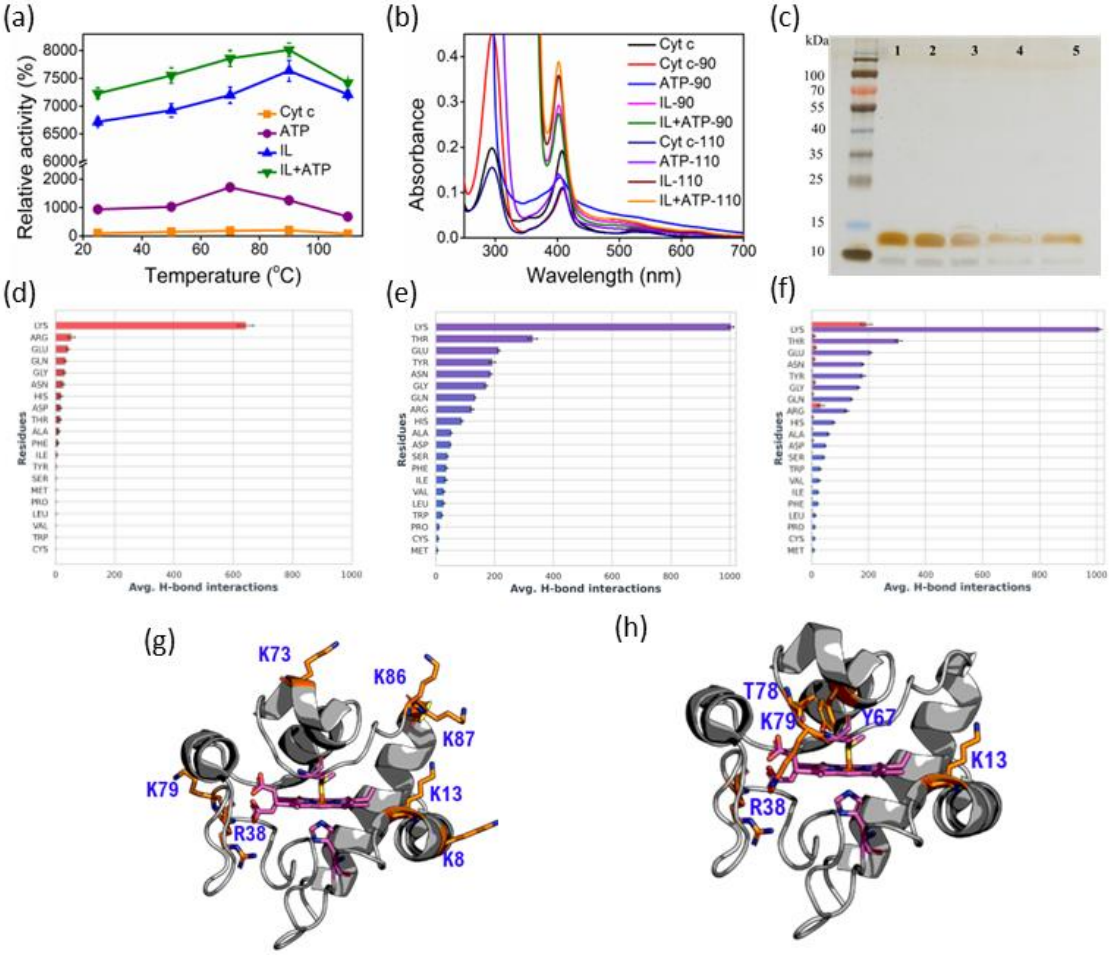

Figure 6: (a) Peroxidase activity of Cyt c with and without nano-structured hydrotropes at different temperatures. (b) UV-vis spectra of Cyt c at higher temperatures (90°C and 110°C) with and without nano-structured hydrotropes. (c) SDS-PAGE image of native Cyt c (lane 1), Cyt c incubated at 100°C (lane 2), Cyt c + ATP incubated at 100°C (lane 3), Cyt c + [Cho][Sal] incubated at 100°C (lane 4), and Cyt C + ATP + [Cho][Sal] incubated at 100°C (lane 5). (d-f) H-bonding interaction counts of individual residue types obtained from adaptive simulation data of Cyt c in the presence of ATP (d), IL (e), ATP and IL in the ATP+IL system (f) are depicted with ATP in red and IL in blue. All simulations were performed at 90°C. (g, h) Plot depicts the position of residues having a higher occurrence of H-bonding with ATP (g) and IL (h), respectively. In all cases, the concentration of ATP and IL was 5 mM and 300 mg/mL, respectively.

A systematic computational study was undertaken at 90°C to gain structural insights into the higher stability of nano-structured-caged Cyt c at elevated temperatures. As expected, the Cyt c conformational ensemble was significantly altered at the higher temperature, with backbone RMSD being approximately 3-4 times higher than that of at 26.85°C for all four solvents (Figure S12a). No significant effects were observed between the mobility of the Ω 40-54 residue region in the four systems than that observed for 26.85°C (Figure 4e and S12b). However, the thermal stability of the Ω 70-85 residues region was significantly enhanced with nano-structured hydrotropes compared to

water (Figure S12b). From Bayesian Markov state models constructed based on the high-temperature simulations (Figure S12c-f), we could observe that Cyt c in water exhibited severe conformational instability, underlined by a very high RMSD of the open state, as well as the presence of multiple secondary open-like states (Figure S13). In contrast, the presence of ATP or/and IL restricted the maximal range of displacements of the Cyt c backbone, providing heightened Cyt c resistance. Notably, the IL stabilized Cyt c in its closed state, particularly when mixed with ATP (Figure S13). Hence, it is evident that ATP and IL could thermally stabilize the functional component of Cyt c via multiple polar interactions.[24] Affinity of hydrotrope molecules towards specific amino acids at the higher temperature (Figures 6d-h and Figure S14) was found to be similar to that observed at 26.85°C (Figures S14 & S11). Overall, Lys and Arg were found to have frequent H-bonding at 90°C to ATP (Figures 6d, f,g). Similarly to the lower temperature environment, the IL had a broader range of specificity, and more affinity with Lys and Tyr in terms of H-bonding (Figures 6e,f,h). The highest affinity was seen towards K8, K13, R38, K39, K73, K86, and K87 with ATP (Figure 6g), and K13, R38, Y67, T78, and K79 with IL (Figure 6h), all of which are crucial in maintaining thermal stability.[38]

Improved stability of nano-structured hydrotrope-caged Cyt c when exposed to chemical denaturants

Above a particular concentration and on more prolonged exposure to some chaotropic chemicals like H_2O_2, guanidine hydrochloride (GuHCl), and urea cause amide bond disruption or overexpose the metallic core of the enzyme, causing a loss of structural integrity and function. To shield the Cyt c against such chemical denaturants, the protein was incubated with the three nano-structured hydrotropic systems for 10 mins, followed by the addition of a chemical denaturant. After the interaction with 6 M GuHCl for 15 mins, there was a complete disruption in the heme pocket of native Cyt c and the activity severely declined, with the remaining activity approximately ~20%. Conversely, hydrotrope-caged Cyt c maintained initial activity of 8.5-fold, 63-fold, and 66-fold in the presence of ATP, IL, and ATP+IL, respectively (Figure 7a). While urea is known to be a hydrotrope, it is well recognized as a chemical denaturant at concentrations above 6 M. In the pre-denaturation concentrations of urea (1-6 M), a ~30 fold increase in peroxidase-like activity was obtained for Cyt c.[39] After 30 mins incubation with 8 M urea, its activity was recorded at approximately 70% of the initial activity, while IL and ATP+IL hydrotrope-stabilized Cyt c showed similar activity (Figure 7b). Native Cyt c showed a denaturing pattern in the UV-vis spectra with GuHCl (Figure 7c), where the Q band structure was entirely lost and the Soret band was severely blue-shifted. In the case of ATP, changes in the 280 nm shoulder peak suggest partial dissociation of aromatic residues like Tyr and Trp.

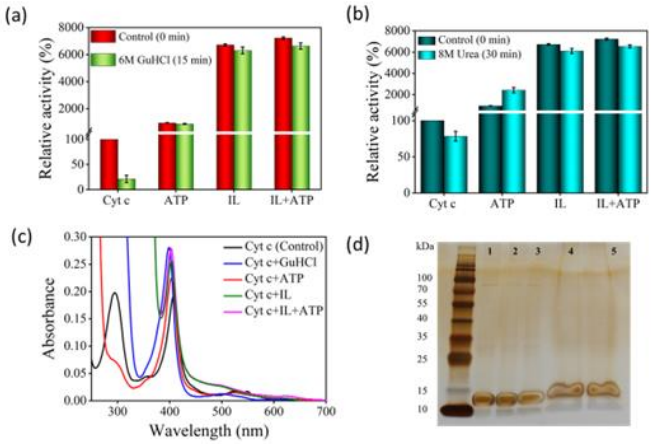

Figure 7: Effect of chemical denaturants, 6 M GuHCl (a) and 8 M urea (b) on the peroxidase activity of Cyt c and nano-structured hydrotrope-caged Cyt c. (c) UV-vis spectra of Cyt c after incubation with 6 M GuHCl. (d) SDS-PAGE image of native Cyt c (lane 1), Cyt c incubated with 8 M urea (lane 2), Cyt c + ATP incubated with 8 M urea (lane 3), Cyt c + [Cho][Sal] incubated with 8 M urea (lane 4), and Cyt c + ATP + [Cho][Sal] incubated with 8 M urea (lane 5). In all cases, the concentration of ATP and IL was 5 mM and 300 mg/mL, respectively.

In contrast, the structures remained almost the same in the cases of IL and ATP+IL, except that the absorbance of the IL-based system trended lower. In the case of ATP, the activity of Cyt c almost doubled (~24-fold higher than native Cyt c) in the presence of urea compared to the Cyt c+ATP system (Figure 7b). This strange observation suggested that ATP cannot prevent the further unfolding of Cyt c in the presence of urea, a behavior confirmed by the UV-vis spectra. For native Cyt c in water, a blue shift similar to GuHCl along with the disruption of the Q band was observed, but for the Cyt c-ATP system, the Q band was retained. The hypochromic shift in the Soret peak for Cyt c-ATP indicated the beginning of structural deformation. IL and ATP+IL followed the regular trend, and this lower activity can be envisioned by the reduced Soret peak intensity (Figure S15). Furthermore, SDS-PAGE analysis demonstrated that Cyt c did not degrade upon treatment with denaturing agents in the presence or absence of ATP and [Cho][Sal] (Figure 7d), thus, confirming that the variation in the activity was due to the changes in the structural conformation of the protein.

Nano-structured hydrotrope-caged Cyt c is resistant to protease digestion

Trypsin, being a proteolytic enzyme, hydrolyses the peptide bond at basic amino acids such as Arg and Lys residues (Figure 8a), thereby denaturing the target protein.[40] Native and hydrotrope-stabilized Cyt c systems were incubated with 6 μM trypsin at 37°C for 24 hr. After the interaction, only 25% of activity was retained for native Cyt c, whereas the hydrotropic systems showed excellent performance

and maintained Cyt c resistant to the action of trypsin (Figure 8b). In the presence of ATP, Cyt c lost only ~2-fold activity compared to activity at the 0 hour (~700% retained), whereas IL and ATP+IL systems retained ~61- and ~67-fold relative activity, respectively. This excellent performance against protease digestion can be deduced by close examination of the interactions of ATP and IL with Cyt c. H-bonding analysis revealed that ATP has a higher tendency to interact with Lys, Arg, and Gln at both 26.85°C and 90°C temperatures, thus suggesting the efficacy of ATP to impart stability to Cyt c (Figures 6d-6g and Figure S12). Additionally, IL also greatly affected the dynamic nature by interacting with a wide range of residues. The affinity of ATP and IL towards Lys and Tyr may be helpful to protect Cyt c by hindering the degradation mechanism of trypsin. The electrostatic and H-bond interactions that occur when Cyt c is nano-structured with ATP completely safeguard the protein from trypsin degradation (Figure 8a). This was further shown by non-reducing SDS-PAGE analysis of the Cyt c before and after digestion with trypsin (Figure 8c). Most of the native Cyt c in the presence of trypsin was found degraded (lane 2, Figure 8c). However, the protein was intact when it was digested in the presence of ATP, IL and a combination of both. From UV-vis spectra (Figure S16), the Q band is lost in almost all the cases (except with ATP) after incubation with trypsin. However, only marginal changes were observed in the Soret band of Cyt c+ATP, and Cyt c+ATP+IL systems, indicating the stability induced by the nano-structured hydrotropes.

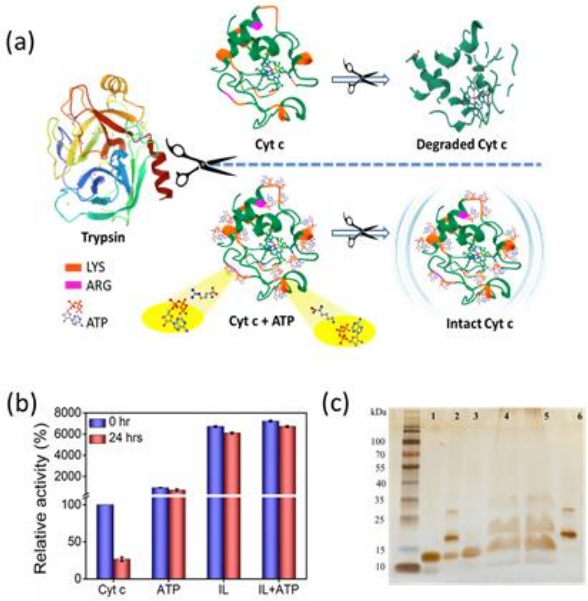

Figure 8: (a) Plausible mechanism of Cyt c digestion in the presence and absence of nano-structured hydrotropes. (b) Effect of protease digestion (6 μM trypsin) on peroxidase activity of Cyt c. (c) SDS-PAGE of native Cyt c (lane 1), Cyt c incubated with trypsin (lane 2), Cyt c + ATP incubated with trypsin (lane 3), Cyt c + [Cho][Sal] incubated with trypsin (lane 4), Cyt C + ATP + [Cho][Sal] incubated with trypsin (lane 5), only trypsin (lane 6). In all cases, the concentration of ATP and IL was 5 mM and 300 mg/mL, respectively.

Nano-structured hydrotrope-caged Cyt c reaction to oxidative stress

Unlike other stress conditions where the peptide backbone is attacked, H_2O_2 initially targets the catalytic site, followed by a breakdown of peptide bonds. Thus, even though H_2O_2 is essential for the peroxidase activity of Cyt c, upon prolonged exposure it causes severe impairment to the protein structure. In our earlier activity studies, 1 mM of H_2O_2 was added at the end, whereas for this study, Cyt c was incubated with H_2O_2 for 30 mins, and the substrate was added afterwards. The activity of bare Cyt c following the induction of oxidative stress was found to be reduced to approximately 60% of its original activity. Conversely, in the presence of ATP, ~219% of activity was retained. This observation can be correlated with the earlier findings in which ATP was found to prevent the oxidation of Cyt c from the Cyt c oxidase enzyme in the mitochondria by hampering the electron flow rate.[41-42] Alternatively, there was a severe drop in the activity of Cyt c from 6700% to just 80% in the presence of IL. These results are not astonishing since the salicylate counterpart is known to enhance the formation of ROS.[22] However, the presence of ATP was found to prevent the oxidation and Cyt c from IL-induced oxidative stress and demonstrated 192% activity. These findings demonstrate the stabilizing effect of nano-structured ATP surrounding Cyt c.

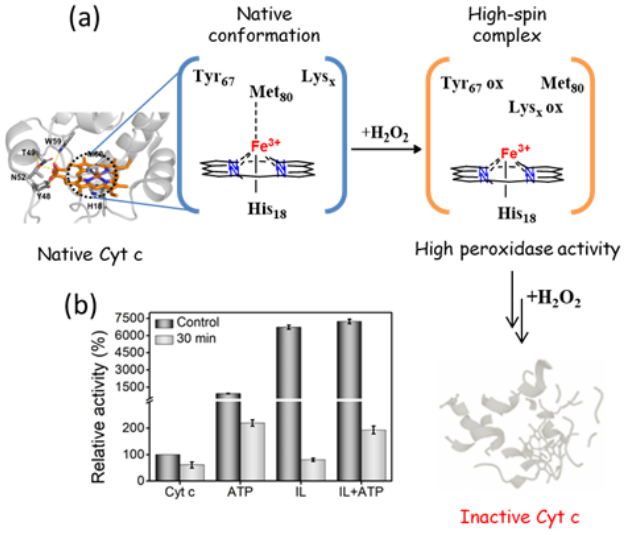

Figure 9: (a) Schematic mechanism showing H_2O_2 induced structural degradation of Cyt c. (b) Effect of H_2O_2 on the peroxidase activity of Cyt c in the presence of different hydrotropes.

CONCLUSIONS

In summary, this study systematically demonstrated the robustness of ATP and IL-based mixed nano-structured

hydrotropes and their utility in the improvement of protein packaging in extreme conditions. From the Mb solubility data, it was shown that the hydrotropic nature of ATP accelerated with the addition of a co-hydrotrope like [Cho][Sal] and vice-versa. Through RDF, DLS, ζ-potential, and UV-vis data, we provided convincing data that ATP forms oligomeric nano-structures at concentrations above 2.5 mM around Cyt c, which can be augmented further with the addition of [Cho][Sal]. A 9-fold increase in peroxidase activity with ATP, 67-fold with IL, and 72-fold with IL+ATP suggested a 'partial reversible unfolding-electrostatic stabilization' mechanism. Reversible binding of ATP and IL with the Ω 40-54 residue loop region of Cyt c showed higher stability at 26.85°C. Moreover, specific binding of nano-structured hydrotropes with Cyt c to Lys and Arg residues through H-bonding and polar interactions with Ω 70-85 region, presented an exceptionally high thermal tolerance with 80-fold activity even at 90°C. Because of such binding specificity, the structure and activity of nano-confined Cyt c were found to be retained against protease digestion, which explicitly cleaves at Lys and Arg residues. Furthermore, ATP and IL-based nano-structured hydrotropes showed efficacy in retaining the functional integrity of Cyt c even in the presence of chemical denaturants like urea and GuHCl, which suggested the suitability of these solvent manipulation strategies for industrial biocatalysis. Through oxidative stress studies, a stark observation was made where [Cho][Sal] was found to enhance ROS formation, which could be efficiently subdued by adding ATP. These results have the potential for counteracting oxidative stress inside the living cells. Thus, the novel strategy of protein confinement in nano-structured hydrotropes can find significant usage in protein packaging under biotic and abiotic stresses, high-temperature bio-catalysis, and plant cell protection against ROS.

EXPERIMENTAL SECTION

Materials and characterization techniques, IL synthesis, Mb solubility study, and SDS-PAGE analysis details are provided in supporting information.

Peroxidase activity of Cyt c at room temperature and under harsh conditions: For activity profiling, a standard ABTS assay was employed where ABTS (3 mM) is oxidized to $ABTS^{+\bullet}$ in the presence of H_2O_2 (1 mM) and catalyzed by Cyt c (2 μM). All chemicals were kept at 25°C for an hour, followed by the incubation of Cyt c with different concentrations of ATP, IL, and IL+ATP for 10 mins. With the addition of ABTS and peroxide, the green color of ABTS intensifies due to the formation of cationic radicals, and variation of absorbance at 420 nm was monitored for 60 seconds with 1-sec intervals, resulting in a straight line. For the temperature studies, Cyt c alone, or incubated with hydrotropic systems were allowed to attain room temperature after subsequent heating (from 25-110°C for 30 mins). For chemical denaturants, 8 M of urea and 6 M of GuHCl were added to the native and pre-incubated catalytic systems, and the activity was checked at 30 and 15 mins, respectively. To profile the activity of Cyt c in the presence of a biological denaturant, the protein with and without hydrotropes was further incubated with 6 μM of trypsin at 37°C for 24 hrs. Finally, for oxidative stress examination, all systems were incubated with H_2O_2 for 15 mins, followed by the addition of ABTS. For all the activity studies, the slope of the curve obtained for native Cyt c was taken as 100%, and the activity of other systems was calculated relative to this.

System setup and Molecular Dynamics simulation: The input model was based on the crystallographic structure of bovine heart Cyt c (PDB code: 2B4Z) at 1.5 Å resolution. The force field parameters for the heme cofactor were produced following a literature search for which the geometry optimization was done using the Gaussian 16 program.[43] All the simulations were established using the AMBER 18 platform[44], and the parameters for ATP were retrieved from the AMBER parameter database.[45] Structures of [Cho][Sal] were obtained from the PubChem database (CID 54686350), and the force field parameters were generated using the Antechamber program and General Amber Force Field - GAFF2 charges.[46-47] Four molecular systems were prepared, keeping the protein Cyt c in water, ATP, IL, and both ATP and IL. All molecular systems were solvated in a cubic box with a side length of 10 nm prepared using a PACKMOL package.[29] The number of ATP molecules corresponds to the concentration of 5 mM, which is 3 ATP molecules, and the number of IL corresponds to 300 mg/mL with a total of 350 molecules of [Cho][Sal]. The protein was modeled using the AMBER ff19SB force field.[48] The protein structure was further protonated using H++ web server pH 6.8.[49] The protein complexes were solvated using OPC water models and then neutralized with counter ions (Na^+ and Cl^-) to achieve the ionic strength of 0.1 M. The systems were then minimized using PMEMD and PMEMD.CUDA modules[50] of AMBER 18 and equilibrated under constant pressure and temperature (NPT) conditions at 1 atm and 300 K using the Langevin thermostat and periodic boundary conditions using the particle mesh Ewald method[51] with 4 fs time-steps enabled by SHAKE and hydrogen mass repartitioning algorithms.[52] Using the steepest descent minimization method, the systems were minimized for several rounds with decreasing harmonic restraints. The following steps included continued heating of the systems from 200 K to 300 K with restraints on only the heavy atoms for 1 ns, followed by NPT equilibration with backbone restraints for 1 ns. Finally, the production run was performed using several rounds of unrestrained NPT simulations with a frame saving rate of 200 ps and total sampling time of 1 ns at constant temperature and pressure using the weak-coupling barostat and thermostat.[53] The final configurations of protein in different solvent en-

vironments were adopted for simulations at room temperature (300 K; 26.85°C) and higher temperatures (363.15 K; 90°C). The last snapshots from the production run were used for the initial input structure for adaptive sampling simulations using the High-Throughput Molecular Dynamics (HTMD) package.[54] The dihedral angle of the protein backbone was defined as the guiding matrix in adaptive sampling simulations. A total of 10 epochs were sampled, with each epoch consisting of 10 individual simulations of 100 ns, totaling 10 µs. All the trajectories were analyzed using the cpptraj program and its Python front-end, pytraj. [55] Further classical MD of 200 ns lengths were performed for solvent systems of ATP, IL, and both ATP and IL without protein.

***Markov state models*:** The Markov state models (MSM) were obtained using the functionalities of the pyEMMA program implemented in the HTMD protocol.[56] The high dimensionality space was reduced using time-lagged independent component analysis (TICA). The models were generated, and the number of metastable states was selected based on the spectral separation analysis (Figures S17 & S18). A lag time of 40 ns was chosen to estimate the final Markov model (Figures S19 & S20).

ASSOCIATED CONTENT

Supporting Information - Details of materials and methods, experimental processes, and figures related to DLS, zeta potential, UV-vis, and computational results have been provided. "This material is available free of charge via the Internet at http://pubs.acs.org." The parameters and input files for MD simulations variants, the key restart files, representative conformations of metastable states, and raw outputs from analyses are freely available at https://doi.org/10.5281/zenodo.7602239.

AUTHOR INFORMATION

Corresponding Authors

GF: fgre@igr.poznan.pl;
JB: janbre@amu.edu.pl; jbrezovsky@iimcb.gov.pl
DM: dmtapu@gmail.com; dmon@igr.poznan.pl

ACKNOWLEDGMENT

D.M. acknowledges SERB, India (EEQ/2021/000059), for the research grant. D.K.S. was a recipient of a scholarship provided by POWER project POWR.03.02.00-00-I006/17. The computations were performed at the Poznan Supercomputing and Networking Center. D.M. and G.F. acknowledge the NANOPLANT project, which received funding from the European Union's Horizon 2020 research and innovation program under grant agreement no. 856961.

REFERENCES

1. Eguchi, Y.; Srinivasan, A.; Tomaselli, K. J.; Shimizu, S.; Tsujimoto, Y. ATP-dependent steps in apoptotic signal transduction. *Cancer Res.* **1999**, *59*, 2174.
2. Fyodorov, D. V.; Kadonaga, J. T. Dynamics of ATP-dependent chromatin assembly by ACF. *Nature.* **2002**, *418*, 896.
3. Hochstrasser, M.; Wang, J. Unraveling the means to the end in ATP-dependent proteases. *Nat. Struct. Biol.* **2001**, *8*, 294.
4. Lee, S.-J. α-Synuclein aggregation: a link between mitochondrial defects and Parkinson's disease? *Antioxid. Redox Signal.* **2003**, *5*, 337.
5. Patel, A.; Malinovska, L.; Saha, S.; Wang, J.; Alberti, S.; Krishnan, Y.; Hyman, A. A. ATP as a biological hydrotrope. *Science.* **2017**, *356*, 753.
6. Neuberg, C. Hydrotropy. *Biochem. Z.* **1916**, *76*, 107.
7. Werner, K.; Krister, H.; Thomas, Z. Hydrotropes. *Curr. Opin. Colloid Interface Sci.* **2016**, *22*, 99.
8. Mei, D.; Jian, K.; Liangzhong, L.; Yifan, L.; Lu, W.; Jianxing, S. ATP is a cryptic binder of TDP-43 RRM domains to enhance stability and inhibit ALS/AD-associated fibrillation. *Biochem. Biophys. Res. Commun.* **2020**, *522*, 247.
9. Jack, V. G.; Thomas, G. Hydrotropic function of ATP in the crystalline lens. *Exp. Eye Res.* **2020**, *190*, 107862.
10. Nishizawa, M.; Walinda, E.; Morimoto, D.; Kohn, B.; Scheler, U.; Shirakawa, M.; Sugase, K. Effects of weak nonspecific interactions with ATP on proteins. *J. Am. Chem. Soc.* **2021**, *143*, 11982.
11. Sarkar, S.; Mondal, J. Mechanistic Insights on ATP's Role as a Hydrotrope. *J. Phys. Chem. B.* **2021**, *125*, 7717.
12. Johannes, M.; Tuan-Minh, D.; Didier, T.; Max, H.; Ali, K.; Dominik, H.; Werner, K. Hofmeister versus Neuberg: is ATP really a biological hydrotrope? *Cell Rep. Phys. Sci.* **2021**, *2*, 100343.
13. Ou, X.; Lao, Y.; Xu, J.; Wutthinitikornkit, Y.; Shi, R.; Chen, X.; Li, J. ATP Can Efficiently Stabilize Protein through a Unique Mechanism. *JACS Au.* **2021**, *1*, 1766.
14. Jiang, H. J.; Atkin, R.; Warr, G. G. Nanostructured ionic liquids and their solutions: Recent advances and emerging challenges. *Curr. Opin. Green Sustain. Chem.* **2018**, *12*, 27.
15. Sindhu, A.; Kumar, S.; Mondal, D.; Bahadur, I.; Venkatesu, P. Protein packaging in ionic liquid mixtures: an ecofriendly approach towards the improved stability of β-lactoglobulin in cholinium-based mixed ionic liquids. *Phys. Chem. Chem. Phys.* **2020**, *22*, 14811.
16. Sintra, T. E.; Abranches, D. O.; Benfica, J.; Soares, B. P.; Ventura, S. P. M.; Coutinho, J. A. P. Cholinium-based ionic liquids as bioinspired hydrotropes to tackle solubility challenges in drug formulation. *Eur. J. Pharm. Biopharm.* **2021**, *164*, 86.
17. Greaves, T. L.; Drummond, C. J. Solvent nanostructure, the solvophobic effect and amphiphile self-assembly in ionic liquids. *Chem. Soc. Rev.* **2013**, *42*, 1096.
18. Bui-Le, L.; Clarke, C. J.; Bröhl, A.; Brogan, A. P. S.; Arpino, J. A. J.; Polizzi, K. M.; Hallett, J. P. Revealing the complexity of ionic liquid–protein interactions through a multi-technique investigation. *Commun. Chem.* **2020**, *3*, 55.
19. Hayes, R.; Warr, G. G.; Atkin, R. Structure and nanostructure in ionic liquids. *Chem. Rev.* **2015**, *115*, 6357.
20. Sanchez-Fernandez, A.; Leung, A. E.; Kelley, E. G.; Jackson, A. J. Complex by design: Hydrotrope-induced micellar growth in deep eutectic solvents. *J. Colloid Interface Sci.* **2021**, *581*, 292.
21. Xie, Z.; Chen, Z. Salicylic acid induces rapid inhibition of mitochondrial electron transport and oxidative phosphorylation in tobacco cells. *Plant Physiol.* **1999**, *120*, 217.
22. Poór, P. Effects of salicylic acid on the metabolism of mitochondrial reactive oxygen species in plants. *Biomolecules.* **2020**, *10*, 341.
23. Martínez-Reyes, I.; Chandel, N. S. Mitochondrial TCA cycle metabolites control physiology and disease. *Nat. Commun.* **2020**, *11*, 102.
24. Alvarez-Paggi, D.; Hannibal, L.; Castro, M. A.; Oviedo-Rouco, S.; Demicheli, V.; Tórtora, V.; Tomasina, F.; Radi, R.; Murgida,

D. H. Multifunctional cytochrome c: learning new tricks from an old dog. *Chem. Rev.* **2017**, *117*, 13382.
25. Shet, S. M.; Bharadwaj, P.; Bisht, M.; Pereira, M. M.; Thayallath, S. K.; Lokesh, V.; Franklin, G.; Kotrappanavar, N. S.; Mondal, D. Presenting B-DNA as macromolecular crowding agent to improve efficacy of cytochrome c under various stresses. *Int. J. Biol. Macromol.* **2022**, *215*, 184.
26. Chen, Y.; Jiménez-Ángeles, F.; Qiao, B.; Krzyaniak, M. D.; Sha, F.; Kato, S.; Gong, X.; Buru, C. T.; Chen, Z.; Zhang, X.; Gianneschi, N. C.; Wasielewski, M. R.; Olvera de la Cruz, M.; Farha, O. K. Insights into the enhanced catalytic activity of cytochrome c when encapsulated in a metal–organic framework. *J. Am. Chem. Soc.* **2020**, *142*, 18576.
27. Shet, S. M.; Thayallath, S. K.; Bisht, M.; Pereira, M. M.; Coutinho, J. A. P.; Sanna Kotrappanavar, N.; Mondal, D. Engineering, Engineering cytochrome c with quantum dots and ionic liquids: A win-win strategy for protein packaging against multiple stresses. *ACS Sustain. Chem. Eng.* **2021**, *9*, 8327.
28. Aurora, M.; Ileana, C.; Gheorghe, T.; Liviu-Dorel, B.; Ossi, H.; Maria, T.-C. Self-assembly characteristics of gold nanoparticles in the presence of cysteine. *Colloids Surf. A Physicochem. Eng.* **2009**, *338*, 93.
29. Allouche, A.-R. Gabedit—A graphical user interface for computational chemistry softwares. *J. Comput. Chem.* **2011**, *32*, 174.
30. Gomes, I.; Santos, N. C.; Oliveira, L. M. A.; Quintas, A.; Eaton, P.; Pereira, E.; Franco, R. Probing surface properties of cytochrome c at Au bionanoconjugates. *J. Phys. Chem. C.* **2008**, *112*, 16340.
31. Singh, U. K.; Kumari, M.; Khan, S. H.; Bohidar, H. B.; Patel, R. Engineering, Mechanism and dynamics of long-term stability of cytochrome c conferred by long-chain imidazolium ionic liquids at low concentration. *ACS Sustain. Chem. Eng.* **2018**, *6*, 803.
32. Yin, V.; Shaw, G. S.; Konermann, L. Cytochrome c as a peroxidase: activation of the precatalytic native state by H2O2-induced covalent modifications. *J. Am. Chem. Soc.* **2017**, *139*, 15701.
33. Kagan, V. E.; Tyurin, V. A.; Jiang, J.; Tyurina, Y. Y.; Ritov, V. B.; Amoscato, A. A.; Osipov, A. N.; Belikova, N. A.; Kapralov, A. A.; Kini, V.; Vlasova, I. I.; Zhao, Q.; Zou, M.; Di, P.; Svistunenko, D. A.; Kurnikov, I. V.; Borisenko, G. G. Cytochrome c acts as a cardiolipin oxygenase required for release of proapoptotic factors. *Nat. Chem. Biol.* **2005**, *1*, 223.
34. Bushnell, G. W.; Louie, G. V.; Brayer, G. D. High-resolution three-dimensional structure of horse heart cytochrome c. *J. Mol. Biol.* **1990**, *214*, 585.
35. Lambeth, J. D. Cytochrome P-450scc. Cardiolipin as an effector of activity of a mitochondrial cytochrome P-450. *J. Biol. Chem.* **1981**, *256*, 4757.
36. McClelland, L. J.; Mou, T.-C.; Jeakins-Cooley, M. E.; Sprang, S. R.; Bowler, B. E. Structure of a mitochondrial cytochrome c conformer competent for peroxidase activity. *Proc. Natl. Acad. Sci. U.S.A.* **2014**, *111*, 6648.
37. San Francisco, B.; Bretsnyder, E. C.; Kranz, R. G. Human mitochondrial holocytochrome c synthase's heme binding, maturation determinants, and complex formation with cytochrome c. *Proc. Natl. Acad. Sci. U.S.A.* **2013**, *110*, E788.
38. Sato, W.; Hitaoka, S.; Inoue, K.; Imai, M.; Saio, T.; Uchida, T.; Shinzawa-Itoh, K.; Yoshikawa, S.; Yoshizawa, K.; Ishimori, K. Energetic Mechanism of Cytochrome C-Cytochrome c Oxidase Electron Transfer Complex Formation under Turnover Conditions Revealed by Mutational Effects and Docking Simulation. *J. Biol. Chem* **2016**, *291* (29), 15320–15331.
39. Nataša, T.; Rastislav, V.; Veronika, L.; Andrej, M.; Erik, S. Peroxidase activity of cytochrome c in its compact state depends on dynamics of the heme region. *Biochim. Biophys. Acta - Proteins Proteom.* **2018**, *1866*, 1073.
40. Krieger, M.; Kay, L. M.; Stroud, R. M. Structure and specific binding of trypsin: comparison of inhibited derivatives and a model for substrate binding. *J. Mol. Biol.* **1974**, *83*, 209.
41. Smith, L.; Davies, H. C.; Nava, M. E. Effect of adenosine 5'-triphosphate and adenosine 5'-diphosphate on the oxidation of cytochrome c by cytochrome c oxidase. *Biochemistry.* **1980**, *19*, 1613.
42. Craig, D. B.; Wallace, C. J. A. ATP binding to cytochrome c diminishes electron flow in the mitochondrial respiratory pathway. *Protein Sci.* **1993**, *2*, 966.
43. Ahn, S.-H.; Seitz, C.; Cruzeiro, V. W. D.; McCammon, J. A.; Götz, A. W. Data for molecular dynamics simulations of Escherichia coli cytochrome bd oxidase with the Amber force field. *Data Br.* **2021**, *38*, 107401.
44. DA, C.; Ben-Shalom, S.; Brozell, D.; Cerutti III, T.; Cheatham III, V.; Cruzeiro, T.; Darden, R.; Duke, D. G.; Gilson, M.; Gohlke, H. AMBER 18. *UCSF.* **2018**.
45. Meagher, K. L.; Redman, L. T.; Carlson, H. A. Development of polyphosphate parameters for use with the AMBER force field. *J. Comput. Chem.* **2003**, *24*, 1016.
46. Junmei, W.; Wei, W.; Peter, A. K.; David, A. C. Automatic atom type and bond type perception in molecular mechanical calculations. *J. Mol. Graph. Model.* **2006**, *25*, 247.
47. He, X.; Man, V. H.; Yang, W.; Lee, T.-S.; Wang, J. A fast and high-quality charge model for the next generation general AMBER force field. *J. Chem. Phys.* **2020**, *153*, 114502.
48. Tian, C.; Kasavajhala, K.; Belfon, K. A. A.; Raguette, L.; Huang, H.; Migues, A. N.; Bickel, J.; Wang, Y.; Pincay, J.; Wu, Q.; Simmerling, C. ff19SB: Amino-acid-specific protein backbone parameters trained against quantum mechanics energy surfaces in solution. *J. Chem. Theory Comput.* **2020**, *16*, 528.
49. Anandakrishnan, R.; Aguilar, B.; Onufriev, A. V. H++ 3.0: automating p K prediction and the preparation of biomolecular structures for atomistic molecular modeling and simulations. *Nucleic Acids Res.* **2012**, *40*, W537.
50. Götz, A. W.; Williamson, M. J.; Xu, D.; Poole, D.; Le Grand, S.; Walker, R. C. Routine microsecond molecular dynamics simulations with AMBER on GPUs. 1. Generalized born. *J. Chem. Theory Comput.* **2012**, *8*, 1542.
51. Zwanzig, R. Nonlinear generalized Langevin equations. *J. Stat. Phys.* **1973**, *9*, 215.
52. Hopkins, C. W.; Le Grand, S.; Walker, R. C.; Roitberg, A. E. Long-time-step molecular dynamics through hydrogen mass repartitioning. *J. Chem. Theory Comput.* **2015**, *11*, 1864.
53. Berendsen, H. J. C.; Postma, J. P. M.; Gunsteren, W. F. v.; DiNola, A.; Haak, J. R. Molecular dynamics with coupling to an external bath. *J. Chem. Phys.* **1984**, *81*, 3684.
54. Doerr, S.; Harvey, M. J.; Noé, F.; De Fabritiis, G. HTMD: high-throughput molecular dynamics for molecular discovery. *J. Chem. Theory Comput.* **2016**, *12*, 1845.
55. Roe, D. R.; Cheatham, III, T. E. PTRAJ and CPPTRAJ: Software for Processing and Analysis of Molecular Dynamics Trajectory Data. *J. Chem. Theory Comput.* **2013**, 9, 3084.
56. Scherer, M. K.; Trendelkamp-Schroer, B.; Paul, F.; Pérez-Hernández, G.; Hoffmann, M.; Plattner, N.; Wehmeyer, C.; Prinz, J.-H.; Noé, F. PyEMMA 2: A software package for estimation, validation, and analysis of Markov models. *J. Chem. Theory Comput.* **2015**, *11*, 5525.